THE SEISMOLOGICAL SOCIETY OF AMERICA
400 Evelyn Ave., Suite 201
Albany, CA 94706-1375
(510) 525-5474; FAX (510) 525-7204
www.seismosoc.org

Bulletin of the Seismological Society of America, Vol. 107, No. 4, pp. 1849–1859, August 2017, doi: 10.1785/0120160296

The Potential of High-Rate GPS for Strong Ground Motion Assessment

by Clotaire Michel, Krisztina Kelevitz,* Nicolas Houlié,* Benjamin Edwards, Panagiotis Psimoulis, Zhenzhong Su, John Clinton, and Domenico Giardini

Abstract We show that high-rate Global Positioning System (GPS) can have a vital role to play in near-real-time monitoring of potentially destructive earthquakes. We do this by investigating the potential of GPS in recording strong ground motions from earthquakes in Switzerland and Japan. The study uses finite-fault stochastic ground-motion simulation based on Fourier amplitude spectra and duration models previously developed for both countries, allowing comparisons in terms of both Fourier and time-domain characteristics (here, the peak ground velocity [PGV]).

We find that earthquakes of magnitude $M_w > 5.8$ can be recorded by GPS in real time at 10 km distance, that is, their Fourier spectrum exceeds the noise of the instruments enough to be used in strong-motion seismology. Postprocessing of GPS time series lowers the noise and can improve the minimum observable magnitude by 0.1–0.2. As GPS receivers can record at higher rates (> 10 Hz), we investigate which sampling rate is sufficient to optimally record earthquake signals and conclude that a minimum sampling rate of 5 Hz is recommended. This is driven by recording events at short distances (below 10 km for magnitude 6 events and below 30 km for magnitude 7 events).

Furthermore, the maximum ground velocity derived from GPS is compared with the actual PGV for synthetic signals from the stochastic simulations and the 2008 M_w 6.9 Iwate earthquake. The proposed model, confirmed by synthetic and empirical data, shows that a reliable estimate of PGV for events of about magnitude 7 and greater can be basically retrieved by GPS in real time and could be included, for instance, in ShakeMaps for aiding postevent disaster management.

Introduction

In earthquake engineering, understanding the seismic ground motion at intermediate and long periods ($T > 0.5$ s) is useful to estimate the nonlinear response of large structures, such as long bridges or tall buildings, to earthquakes (Cauzzi and Faccioli, 2008). Among the available intensity measures (IMs) describing ground motion, peak ground velocity (PGV) is popular and relates to intermediate periods (0.5–3 s, Bommer and Alarcon, 2006; Bradley, 2012). PGV correlates well with damage to structures and macroseismic intensity (Faenza and Michelini, 2010; Lesueur *et al.*, 2013) and therefore it has been adopted as the main parameter used in ShakeMap for conversion of instrumental ground motion to macroseismic intensity (Worden *et al.*, 2010; Cauzzi *et al.*, 2015). It is also a good indicator of the occurrence of soil liquefaction (Orense, 2005) and damage to particular infrastructure, such as pipe networks (Jeon and O'Rourke, 2005). Although neglected in the last decades, most recent ground-motion prediction equations (GMPEs) now predict PGV (Akkar *et al.*, 2014). Although some GMPEs include long-period broadband records (Cauzzi and Faccioli, 2008), a general lack of data at long periods means that such models are still not able to accurately predict the associated IMs. This lack of data is due to the limited number of high-quality long-period recordings in the near field of large earthquakes. This is because weak-motion broadband seismometers saturate at 1.3 cm/s, a value routinely exceeded in the near field of even moderate M_w 4 earthquakes (Hauksson *et al.*, 2001), and strong-motion accelerometers have unstable performance at long periods (Bommer and Alarcon, 2006; Cauzzi and Faccioli, 2008; Cauzzi *et al.*, 2015; Ibrahim *et al.*, 2016). Indeed, depending on the quality of the site and the installation, modern strong-motion stations may provide very accurate long-period records of earthquakes, though any tilting or rotation associated with the ground motion will make the record difficult to interpret at long periods. To date, no GMPE includes long-period records collected by Global Positioning System (GPS) networks.

*Also at Mathematical Physical Geodesy (MPG), ETH Zurich, Robert-Gnehm-Weg 15 8093 Zürich, Switzerland.

Today, the standard sampling rate of Global Navigation Satellite Systems (GNSS) receivers is 1 Hz with some receivers capable of up to 100 Hz (Häberling *et al.*, 2015). Displacement time series up to 10 Hz have proven to be reliable and could be streamed in real time (Genrich and Bock, 2006; Avallone *et al.*, 2011). Häberling *et al.* (2015) showed that beyond this rate, signal autocorrelation could take place. 1 Hz GPS recordings have been used to detect motions of the Earth's surface associated with seismic-wave propagation (Larson *et al.*, 2003; Houlié *et al.*, 2011; Kaloop and Rabah, 2016), for earthquake early warning (Allen and Ziv, 2011; Bock *et al.*, 2011), to invert for coseismic slip of large ($M_w > 6$) events (Miyazaki *et al.*, 2004; Miyazaki and Larson, 2008; Rhie *et al.*, 2009; Houlié *et al.*, 2014), to constrain seismic moment magnitude (Melgar *et al.*, 2015), and to record the Earth's normal modes (Mitsui and Heki, 2012), or simply coseismic offsets (Larson *et al.*, 2003). Psimoulis *et al.* (2014) showed that it is possible to establish maximum ground velocity (MGV) maps at long periods ($T > 3$ s) using high sampling rate GPS data collected during the 2011 Tohoku-Oki megathrust event. Some deep basins in Japan with a fundamental period of 3 s or more showed large amplifications of the long-period ground motion during the Tohoku-Oki event, which are not taken into account by commonly used high-frequency amplification proxies such as V_{S30}. Although GMPEs established for Japan (Zhao *et al.*, 2006) showed acceptable results for this event, they have been developed without using any data for earthquakes in this magnitude range with such large amplitudes at long periods. Considering that the closest seismic records were onshore at ~75 km from the epicenter, the high-frequency ground motions were already attenuated when reaching the coastline of Japan. Psimoulis *et al.* (2014) showed that the 5% damped pseudospectral acceleration (PSA) at 3 s retrieved with GPS was the same as that retrieved with the accelerometric network, which is a further indication of the capability of GPS data for such events. Because the study of Psimoulis *et al.* (2014) was based on 1 Hz, it was unclear how much of PGV could have been captured by the GNSS Earth Observation Network System (GEONET) running at a higher sampling rate. In the present study, we investigate whether high-rate GPS records are able to, and how reliably they can, quantify "true" broadband PGV. We also determine what sampling rate is optimal to capture the widest range of signal, while not recording sensor noise.

In this article, we first quantified the capabilities of GPS to record ground motion in terms of event size and distance to the source by comparing stochastic ground-motion simulation models for Switzerland and Japan (Edwards and Fäh, 2013; Poggi *et al.*, 2013) with GPS noise obtained with different sampling rates and processing software. Recording capability is meant here in the sense of engineering seismology (high signal-to-noise ratio [SNR] for the amplitude in the Fourier domain), not in the sense of recording a particular phase of the earthquake signal. We further derived waveforms and peak amplitudes from these ground-motion models to estimate what proportion of PGV could be retrieved by GPS and the impact of sampling frequency on this parameter.

Table 1
Parameters Used to Define the Earthquake Fourier Amplitude Spectrum (FAS) for Japan and Switzerland

Parameter	Switzerland	Japan
Source	Brune (1970)	Brune (1970)
Stress drop (MPa)	6.3	10
κ	$0.000238R + 0.017$	$0.000238R + 0.022$
Geometrical decay	$R^{-1.29}$ ($R < 20$ km) $R^{-0.59}$ ($20 < R < 140$ km) $R^{-1.02}$ ($R > 140$ km)	$R^{-1.25}$ ($R < 50$ km) $R^{-1.13}$ ($50 < R < 110$ km) $R^{-1.67}$ ($R > 110$ km)

Data and Models

Stochastic Ground-Motion Models

Stochastic earthquake ground-motion simulation techniques (Boore, 2003) have been widely used to develop regionally calibrated strong ground motion datasets in regions of low-to-moderate seismicity (Atkinson and Boore, 2006; Rietbrock *et al.*, 2013; Cauzzi *et al.*, 2015). They are based on combining earthquake Fourier amplitude spectrum (FAS) models with shaking duration models upon the assumption of random phase acceleration signals (Hanks and Mcguire, 1981). Extended fault models with distributions of discrete point sources have been used to better model the low-frequency radiation (Motazedian and Atkinson, 2005) including directivity.

The advantage of stochastic techniques is that they are based on simple seismological models accounting for source, path, and site effects. They are therefore very computationally efficient. In fact, because many source parameters (e.g., hypocenter on the fault plane, slip distribution) are *a priori* unknown, then simple point-source models with geometrical adjustments for finite-fault effects provide, on average, the same results as models that discretize the fault plane (Atkinson *et al.*, 2009; Boore, 2009). For this study, stochastic simulation models developed for Switzerland (Edwards and Fäh, 2013) and Japan (Poggi *et al.*, 2013) have been used. In the first part of the study, these models are compared with GPS noise spectra. Both models have FAS that are calibrated based on regional seismicity. The parameters controlling the FAS model are stress parameter (Atkinson and Beresnev, 1997), anelastic attenuation κ (Anderson and Hough, 1984), and geometrical decay. The parameters used to define the FAS models are given in Table 1. Moreover, Edwards and Fäh (2013) propose a duration model that depends on magnitude and distance. It is used to convert from FAS to power spectral density (PSD, see the Computation of the PSD Spectra from Time Series section). To include vertical FAS, we implemented the model of Edwards, Poggi, and Fäh

(2011) which combined Swiss and Japanese data to provide a model of the vertical-to-horizontal (V/H) spectral ratio at rock sites for both FAS and response spectra. The model uses the quarter-wavelength shear-wave velocity to determine site-specific estimates of V/H. The computations are performed at the reference rock for Switzerland (Poggi *et al.*, 2011) and Japan (Poggi *et al.*, 2013), respectively, because typical GPS stations are located at rock sites.

These ground-motion models provide ground motion for known reference conditions, and they are based on seismological models and calibrated on data. However, calibration datasets remain limited and stochastic ground-motion models are based on simple rupture models that limit their accuracy for large magnitude events (maximum studied magnitude M_w 7.5) and at long period (maximum period for calibration: ~2 s, with longer periods relying on the physics of the rupture). All considered magnitudes in this article are moment magnitude M_w.

In a second part of the study, we combined the FAS and duration models for Switzerland (Edwards and Fäh, 2013) to generate synthetic stochastic waveforms to study PGV. The stochastic simulation method, as summarized by Boore (2003), has been shown to be successful at predicting strong ground motion peak amplitudes in various applications (peak ground acceleration [PGA], PGV, PSA, etc.; Atkinson and Assatourians, 2015; Goulet *et al.*, 2015). We used the approach of Motazedian and Atkinson (2005) that uses a discretized point-source fault model with dynamic corner frequencies. The method takes a base seismological model for estimating the FAS of earthquake recordings: source type of the subfaults (Brune, 1970) and their stress parameter, the attenuation of energy through the crust (Q, geometrical spreading), and site amplification and attenuation κ_0 (Anderson and Hough, 1984). The crustal and site-specific attenuation characteristics for Switzerland are detailed in Edwards, Fäh, and Giardini (2011). Stress parameters of 3, 6, and 12 MPa (Cauzzi *et al.*, 2015) were used to account for epistemic uncertainties in the source type, whereas κ_0 (Anderson and Hough, 1984) of 0.01, 0.02, and 0.03 s were used to account for variations in site attenuation characteristics. It is possible to vary other seismological parameters, but κ_0 and stress parameter are the most sensitive terms and can be used to account for epistemic uncertainty in extrapolating to large magnitude events (Drouet and Cotton, 2015; Bommer *et al.*, 2016)—which allows us to cover a realistic range of scenarios. Events with M_w 5.5–7.5 were simulated in 0.5 magnitude unit intervals at 5, 10, and 15 km depth, with appropriate fault dimensions (Wells and Coppersmith, 1994). The hypocenter location and slip of scenario earthquakes were randomized and synthetic waveforms were generated. Simulations were produced at distances of 2, 5, 10, 15, 20, 40, 60, 80, and 100 km from the center of the surface projection of the fault strike at 0° (fault parallel), 45°, and 90° azimuth.

The seismicities of Switzerland and Japan are different, so the range of magnitudes and distances of interest for our study are also different. In Switzerland, the maximum magnitude in the earthquake catalog is M_w 6.6, whereas M_w 6.0 events are expected every century (Fäh *et al.*, 2011). The GPS network has interstation distances in the order of 30 km so that we can expect recordings at distances shorter than 15 km. Maximum distances of 200 km are considered in the model of Edwards and Fäh (2013), which corresponds roughly to the size of the country. In Japan, the maximum studied magnitude is limited by the FAS model of Poggi *et al.* (2013), for which ground motion modeled for magnitudes larger than 7.5 are not reliable. The Japanese network extends also over a much larger distance, with recordings of the Tohoku-Oki earthquake at 1000 km distance and with a 30 km spacing.

GPS Noise Data

We computed noise spectra of GPS displacement time series established using various software packages (Bernese, GAMIT, and RTKLIB), GPS datasets from different networks (GNSS Earth Observation Network System [GEONET]; International GNSS Service [IGS]; and station GBN, part of a temporary network deployed in Greece), and processing modes (precise point positioning [PPP], double difference [DD], and real-time kinematic [RTK]) to reveal the noise characteristics for the various processing options. PPP solutions using PPP-Bernese (Dach *et al.*, 2015) and RTKLIB (Takasu *et al.*, 2007) software could have been implemented in near-real-time, as RTNet (Rocken *et al.*, 2004) time series of the Tohoku-Oki event, using orbit and clock products available in real time (i.e., ultra-rapid products) for the GPS data processing. GAMIT solutions however would require some development (such as distribution of processing load) to be computed in near-real-time. One set of solutions (station GBN, Table 2) is measured at 10 Hz, whereas all others are 1 Hz recordings taken before the 2011 Tohoku-Oki and the 2003 Tokachi-Oki (Hokkaido) earthquakes. The 10 Hz dataset allows characterization of the noise of very high-rate GPS data, relative to 1 Hz time series. Characteristics of each GPS dataset are presented in Table 2.

Before going into the details of the data noise analysis, it is useful to highlight differences between the processing techniques. We used both differential processing (RTK and DD) and PPP, and we expect that different techniques would give slightly different results depending on the processing technique used. RTK and DD are differential processing techniques that allow the removal of common errors (ionosphere/troposphere status, orbits errors, clocks errors) over a network. In both cases, the satellite and receiver clock errors are canceled out completely, whereas the orbit errors, ionosphere contribution (all data of L1/L2 type), and troposphere uncertainties are minimized (proportional to the distance between the reference and rover). In applications of GPS in seismology, usually more than two reference stations are selected, which are far from the epicenter and not affected

by the seismic motion. For instance, for the DD solution of the 2003 Tokachi-Oki earthquake, GPS stations located more than 1200 km away from the epicenter that did not experience motions larger than noise level (Kelevitz *et al.*, 2017). Finally, the difference between RTK and DD is that RTK refers to a real-time processing mode, whereas DD is a postprocessing strategy. In postprocessing, the most accurate orbit, ionosphere, and other parameters can be obtained from the IGS, which combines solutions of other GNSS analysis centers (e.g., CODE, GFZ) and provides the highest quality products (Dow *et al.*, 2009) about two weeks after the recording of the data. In contrast, during real-time processing, these parameters are not available and only *a priori* models and approximate information (i.e., broadcast or ultra-rapid products) are used.

The PPP method, however, uses only one station at a time, and therefore the receiver clock bias has to be estimated every epoch as an unknown parameter. For the case of seismic time histories, where we focus on the high-frequency component of the GPS data, the troposphere and orbits are evolving much slower than the ground motion (Houlié *et al.*, 2016) and they are expected to play a minor role in the precision of the retrieved GPS time series.

Because of the different processing techniques, environmental conditions (including multipathing and troposphere state during experiments), and satellite geometry (Houlié *et al.*, 2011), the noise level for each dataset is different (see Fig. 1). The Tokachi-Oki dataset is the most accurate and least noisy dataset because it has been processed with a DD approach (Houlié *et al.*, 2011) using final orbit/clock products. We do not expect to see significant differences in DD mode as implemented in GAMIT, Bernese (Dach *et al.*, 2015), or GIPSY software. Therefore, only GAMIT noise time series are presented to represent the postprocessing mode. The RTK GEONET, PPP GEONET, and GBN solutions are less accurate, as they are either processed in actual real-time conditions (RTK GEONET) or postprocessed in a manner simulating real-time conditions, using the orbit/clock products available for real-time applications. Furthermore, the higher noise of the 10 Hz data relative to 1 Hz GPS data is probably due to the correlated GPS data for high frequencies (i.e., > 1 Hz; Häberling *et al.*, 2015) and the noise of the GPS receiver deployed at the site.

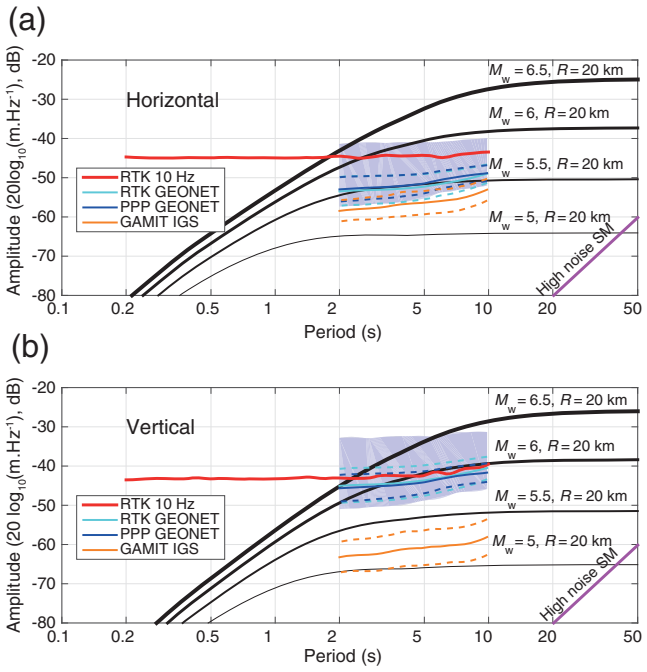

Figure 1. Comparison of displacement spectra of Global Positioning System (GPS) noise series and magnitude 5–6.5 earthquakes at 20 km distance using the Swiss stochastic model (Edwards and Fäh, 2013) for the (a) horizontal and (b) vertical component. The shaded area corresponds to the full range (minimum–maximum of the noise from the 847 precise point positioning [PPP] processed records from the Global Navigation Satellite Systems (GNSS) Earth Observation Network System [GEONET]). Dashed lines correspond to the mean ± one standard deviation. Real-time kinematic (RTK) 10 Hz, RTK GEONET, and GAMIT International GNSS Service (IGS) mean values in the upper plot correspond approximately to noise levels of 14, 2, and 1.2 mm, respectively. The high-noise model for strong-motion (SM) stations (Cauzzi and Clinton, 2013) is the high-noise SM line. The color version of this figure is available only in the electronic edition.

Table 2
Description of the Global Positioning System (GPS) Time Series Used to Compute Noise Spectra

Dataset	Context	Number of Stations	Date (yyyy/mm/dd)	Duration (hr)	Sampling Rate (Hz)	Processing Strategy	Real Time	Software
GBN	Greece; quiet environment	1	2014/09/15	2.5	10	RTK	Simulated	RTKLIB (Takasu *et al.*, 2007)
RTK GEONET	Japan; before 2011 Tohoku-Oki	414	2011/03/11	4	1	RTK	Yes	RTNet
PPP GEONET	Japan; before 2011 Tohoku-Oki	847	2011/03/11	3	1	PPP	Simulated	BERNESE (Dach *et al.*, 2015)
GAMIT IGS	Japan; before 2003 Tokachi-Oki	10	2003/09/24	1.5	1	DD	No	GAMIT (Herring *et al.*, 2015)

DD, double difference; GEONET, GNSS Earth Observation Network System; GNSS, Global Navigation Satellite Systems; IGS, International GNSS Service; PPP, precise point positioning; RTK, real-time kinematic.

Computation of the PSD Spectra from Time Series

The PSD of the GPS noise records is computed using the Welch (1967) method, that is, by computing the average squared Fourier transform of tapered windows normalized by their length. The window size was set to 200 s, which was found to be a good trade-off between the extent in the period range and the accuracy of the average spectrum for the available length of time series (longer than 5400 s; Table 2). A minimum number of 27 windows are therefore available. Periods for which at least 20 cycles are present in a window (i.e., up to 10 s here) are interpreted. The PSDs are then smoothed using the method of Konno and Ohmachi (1998) with a smoothing parameter of 30. For the horizontal components in the following studies, we use the geometric mean.

To be able to compare acceleration models with displacement noise recordings, the conversion from displacement to acceleration (or vice versa) of the FAS is performed by multiplying, or respectively dividing, by $(2\pi f)^2$, in which f denotes the frequency. The FAS as defined by Edwards and Fäh (2013) is the two-sided Fourier transform, which requires therefore an adjustment of a factor of 2 when computing the corresponding PSD. The PSD values are represented in decibels (dB) as $\mathrm{PSD_{dB}} = 10\log_{10}(\mathrm{PSD}) = 10\log_{10}(2\mathrm{FAS}^2/d)$ with d denoting duration, as obtained from the duration model.

Results

Intrinsic Capability of GPS Recordings

We compare the Fourier spectra of the GPS noise recordings with the FAS models for Switzerland (Fig. 1) and Japan (Fig. 2) for typical magnitudes and distances (Switzerland: magnitude 5–6.5, 20 km distance; Japan: magnitude 5.5–7, 100 km distance). Horizontal and vertical components are studied for the Swiss case (Fig. 1). Unlike classical noise comparisons in acceleration, the comparison is performed in displacement units to better accentuate the performance of the GPS.

GPS Noise Levels. Noise of real-time GPS–PPP time series is represented in Figures 1 and 2 by the shaded area that covers the range of the PPP solutions for 847 simultaneous recordings from the Japanese network. It shows a high variability of nearly 20 dB (one order of magnitude). The mean value is located in the lower part of the zone, and one standard deviation is bounded by 6 dB (about a factor of 2), which indicates that the distribution is not symmetric: proportionally fewer recordings have large noise values. Both the distribution of the PPP and RTK solutions are almost identical (5% difference on the mean value) in the horizontal and vertical directions. As expected, the vertical noise is higher than the horizontal. The noise level of the 10 Hz dataset processed with RTK is located in the range of the PPP processing but in the higher part for the horizontal direction (close to the mean for the vertical). Figures 1 and 2 confirm

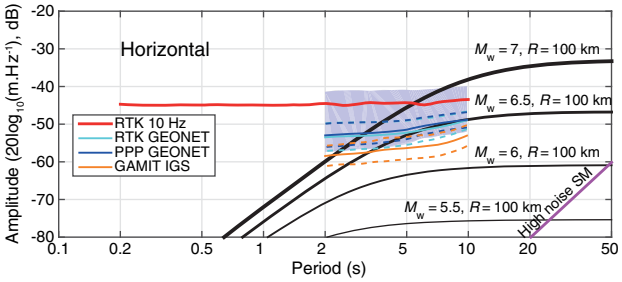

Figure 2. Comparison of displacement spectra of GPS noise series and magnitude 5.5–7 earthquakes at 100 km distance using the Japanese stochastic model (Poggi *et al.*, 2013) for the horizontal components. The shaded area corresponds to the full range (minimum–maximum of the noise from the 847 PPP processing from the GEONET. Dashed lines correspond to the mean ± one standard deviation. The high-noise SM line represents the high-noise model for strong-motion stations (Cauzzi and Clinton, 2013). The color version of this figure is available only in the electronic edition.

that the noise is nearly flat in displacement over the period range, even for higher sampling rates. The postprocessed dataset (GAMIT IGS) shows significantly reduced noise levels (5 dB) in the horizontal direction and extremely reduced noise in the vertical direction (about 20 dB). The variability (standard deviation) is comparable to the PPP but with a symmetric distribution, which means that the few high noise recordings present in the PPP dataset are absent in the GAMIT dataset.

GPS has a relatively flat noise level in displacement over the period (T) range, which means that the GPS noise in velocity is proportional to $1/T$ and to $1/T^2$ in acceleration. The estimation of the PSD is limited at long periods by the window size chosen for the computation, itself limited by the recording duration: we do not consider periods with less than 20 cycles in the time window, that is, 10 s here. At short periods, the PSD estimation is limited by the Nyquist frequency. The noise in the period range where the PSD is reliable, as previously defined, can therefore be approximated with a linear function in log–log scale. We assume that this linear function would extend for longer (if longer noise windows would be used) and shorter periods (if higher sampling rates were used). This assumption has been verified by taking longer time windows and recordings with higher sampling rate.

The high noise model for strong-motion stations of Cauzzi and Clinton (2013) is shown in Figures 1 and 2 to compare the capabilities of high-quality accelerometers. They indicate even a badly performing strong-motion sensor should be more sensitive than GPS at periods at least up to 50 s. In practice though, strong-motion records are contaminated by tilting that greatly increase long-period noise. Careful installation of the strong-motion sensor can avoid local site tilting of the sensor itself or its housing induced by the strong motion, but rotation and tilt associated with the strong ground motion itself cannot easily be removed. Many strong-motion recordings of the Tohoku-Oki event, for

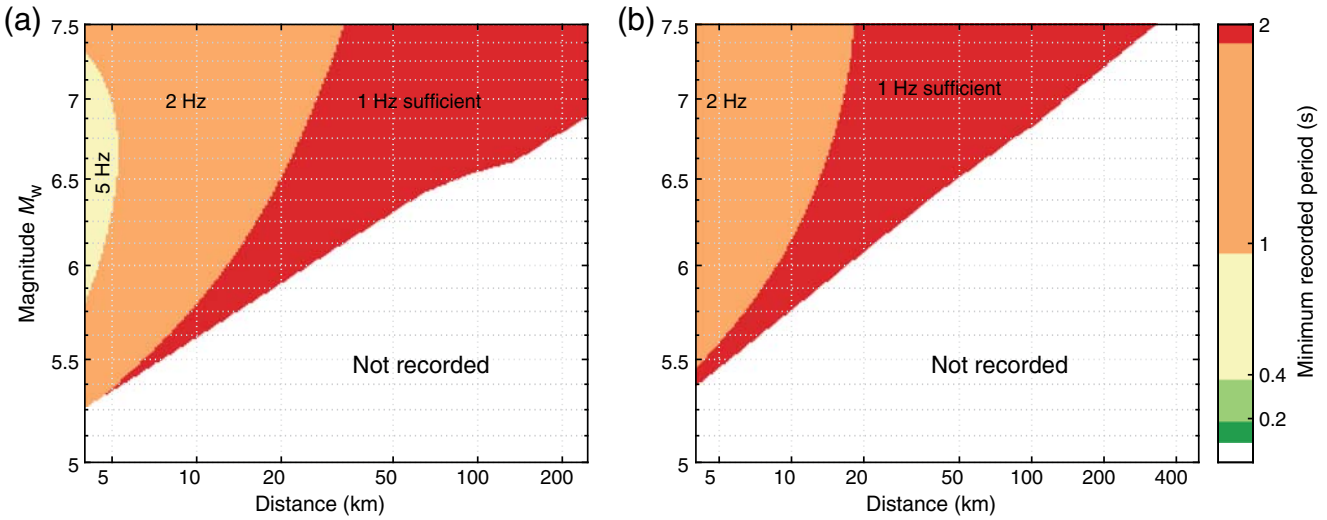

Figure 3. Recording capability of GPS in real-time mode (PPP processing, mean noise level) for (a) Switzerland and (b) Japan. The darker zone is sufficiently recorded by 1 Hz sampling rate GPS, whereas increasing the sampling rate (up to 5 Hz) would be useful to better record the events in the other shaded areas. Note that the distance ranges are different in each case. The color version of this figure is available only in the electronic edition.

instance, exhibit tilting (Psimoulis *et al.*, 2014) that impacts the estimation of ground motion even for periods close to 3 s.

The comparison with the FAS model for earthquake ground motion shows that, for instance, we expect a magnitude 6.5 to be well recorded by GPS on both horizontal and vertical components at periods larger than 2 s at 20 km distance in Switzerland (Fig. 1), whereas a magnitude 5 event cannot be recorded at this epicentral distance with current technology and processing strategies. In the case of the typical 100-km epicentral distance in Japan (Fig. 2), a magnitude 7 should be recorded by GPS above 3 s.

GPS Noise versus Earthquake Spectra. Even for large earthquakes, the amplitude of ground displacement from earthquakes decreases rapidly for shorter periods, and therefore intersects and falls below the resolution of the GPS (Figs. 1 and 2). For the purpose of this study, we define that GPS is able to record an event if the ground motion exceeds the geometric mean of the noise level at long periods by at least a factor of 3 (~10 dB) as commonly assumed (e.g., Edwards *et al.*, 2013). We can then define a minimum period at which the signal can be recorded. This value of 3 is arbitrary though commonly used in seismology, for instance, it is conservative enough to account for the jagged shape of spectra for real events.

The minimum recordable period is useful because it indicates the minimal useful sampling rate. The frequency threshold for which the ground motion exceeds the GPS noise level depends on both the magnitude of the event and the distance to it. Figure 3 summarizes the recording capabilities of GPS in terms of magnitude, distance, and corresponding minimum recorded period, assuming the GPS noise level is given by the mean noise level of the PPP recordings (see Fig. 1), that is, representative of what can be achieved in real time. The unshaded areas correspond to events that cannot be recorded. In the case of Switzerland (Fig. 3a), events of magnitude 5.6 and larger can be recorded on average at 10 km distance, and events of magnitude 6.6 and larger at 100 km distance. Using the minimum and maximum GPS noise levels, at 100 km, the minimum recorded magnitude ranges between 6.4 and 6.9. For Japan (Fig. 3b), magnitude 6.8 events and greater can be recorded at 100 km (min–max [6.7–7.1]), whereas one cannot expect to record events smaller than 7.5 at 300 km distance. The magnitude difference between Switzerland and Japan, controlled by the FAS model, increases from 0.1 at 5 km to 0.3 at 100 km and is due to the stronger attenuation in Japan according to the FAS models.

Improving the minimum event magnitude that can be recorded at a given distance requires decreasing the noise level of the GPS. Postprocessed GPS time series allow a reduction of one order of magnitude (Fig. 4): at 100 km distance, a magnitude 6.4 could then be recorded in Switzerland and a 6.7 in Japan in the horizontal component (a 0.1–0.2 magnitude improvement). These postprocessed data are available for developing ground-motion prediction models but not for real-time applications.

Influence of the Sampling Rate. The minimum period that can be recorded is represented by the shaded areas in Figures 3 and 4. It decreases with the size of the earthquake and increases with distance (the behavior of the sufficient sampling rate is the opposite). The size of the event controls the amplitude of the whole spectrum and therefore the shortest period that can be recorded. Moreover, these short periods are filtered out with increasing distance. Increasing the sampling rate of GPS beyond 1 Hz would therefore improve the

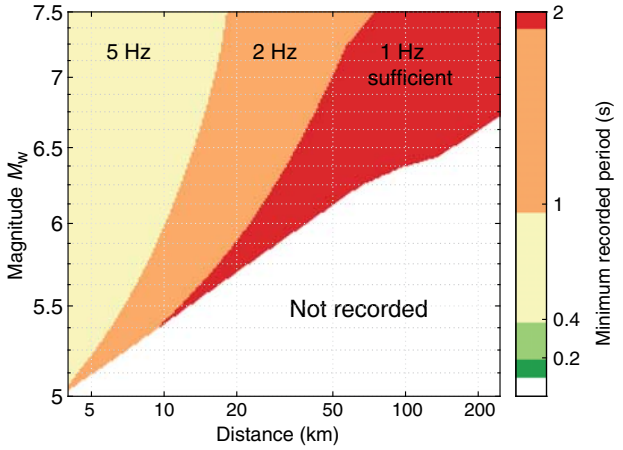

Figure 4. Recording capability of GPS in postprocessing mode (average GAMIT noise level) for Switzerland. Interpretation is same as Figure 3. The color version of this figure is available only in the electronic edition.

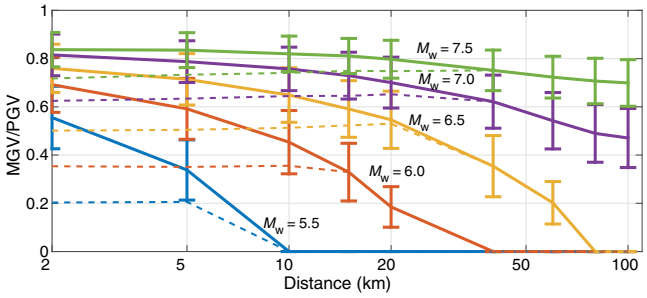

Figure 5. Recording capability of GPS in real-time mode (mean GPS PPP noise level) in terms of retrieval of the peak ground velocity (PGV) value for Switzerland. Maximum ground velocity (MGV)/PGV denotes the ratio between the estimated maximum ground velocity value potentially recorded by a GPS and the actual PGV. Solid lines correspond to a 5 Hz sampling rate, dashed line to a 1 Hz rate. The error bars express the variability due to the used waveforms (different simulation parameters). The color version of this figure is available only in the electronic edition.

recording of earthquakes at short distances, especially large magnitude events.

The current standard sampling rate of 1 Hz, corresponding to (and theoretically including) a 2-s cutoff period filter to avoid aliasing, is sufficient for the magnitude–distance couples displayed in the dark shaded area in Figures 3 and 4 (minimum recorded period of 2 s or larger). Shaded areas other than the darker one indicate that an increase in the GPS sampling rate is required to fully exploit the capability of the GPS for these magnitude/distance combinations. Figure 4 (postprocessing mode) suggests that, for the Swiss model, 1 Hz sampling rate is sufficient to capture motions corresponding to events of magnitudes 5.7 to 5.9 events at 20 km distance, whereas a 2 Hz sampling rate would be useful for larger events. A 5 Hz sampling rate would be sufficient to record all the considered events from 5 km onward. In Japan, the same analysis shows that a sampling rate of 5 Hz is sufficient to capture all available energy from events at 5 km distance and a magnitude up to M_w 7.5. It should however be noticed that the results for large magnitude events (above 7) have not been calibrated with data and should be interpreted with care. Figure 4 shows that a higher sampling rate would be necessary to fully record events in the near field (below 10 km for magnitude 6 events and 30 km for magnitude 7), as also shown by Smalley (2009) using records at 3-km epicentral distance of magnitude M_w 6 and 7.4 earthquakes.

It has been shown (Psimoulis *et al.*, 2014, 2015) that the Tohoku-Oki earthquake had been well recorded above 3 s up to 1000 km distance by GPS instruments. This demonstrates that the 1 Hz sampling frequency (Nyquist frequency of 0.5 Hz or 2 s) is the limiting factor for the period range of observation in this case. Although the Tohoku-Oki event is not covered by our modeling hypotheses, other earthquakes have been well recorded by high-rate GPS (Miyazaki *et al.*, 2004; Bilich *et al.*, 2008; Larson and Miyazaki, 2008; Yokota *et al.*, 2009; Delouis *et al.*, 2010; Shi *et al.*, 2010; Allen and Ziv, 2011; Avallone *et al.*, 2011; Houlié *et al.*, 2011, 2014; Lay *et al.*, 2011; Yue and Lay, 2011; Mitsui and Heki, 2012; Zheng *et al.*, 2012; Kelevitz *et al.*, 2017). A case study is presented in the Observations from the 2008 Iwate–Miyagi Nairiku Earthquake section.

Capability of GPS to Record PGV

We now investigate the capability of GPS to record the PGV in real time. PGV is an important IM for intermediate periods for damage assessment. The quality of the estimate of PGV that can be retrieved with high-rate GPS is therefore a good measure of how useful the recording is for engineering seismology. It is commonly thought that GPS is not able to perform well for this IM. We therefore developed synthetics to show to what extent GPS is capable of recording the true PGV.

As explained in the Stochastic Ground-Motion Models section, for a given magnitude and distance couple, we generate from the Swiss stochastic model (Edwards and Fäh, 2013) a set of synthetic waveforms for different stress drops and κ values. A corresponding set of GPS waveforms are then generated, which accounts for the GPS noise by applying a four-pole low-pass filter at the minimum usable period. We then compute the PGV from the original synthetic waveform and the MGV from the GPS traces. The GPS sampling rate is also simulated with a low-pass filter at the Nyquist frequency: 5 Hz (optimal record of the event) and 1 Hz (typical rate of current networks) are used. In Figure 5, we plot the MGV/PGV ratio for events with magnitudes between 5.5 and 7.5 as a function of distance from the rupture. This ratio decreases with distance: the increasing corner period of the filtering is not compensated by the shift of the frequency content toward longer periods. In the near field, the opposite is true. It can be noticed that the single-station interevent vari-

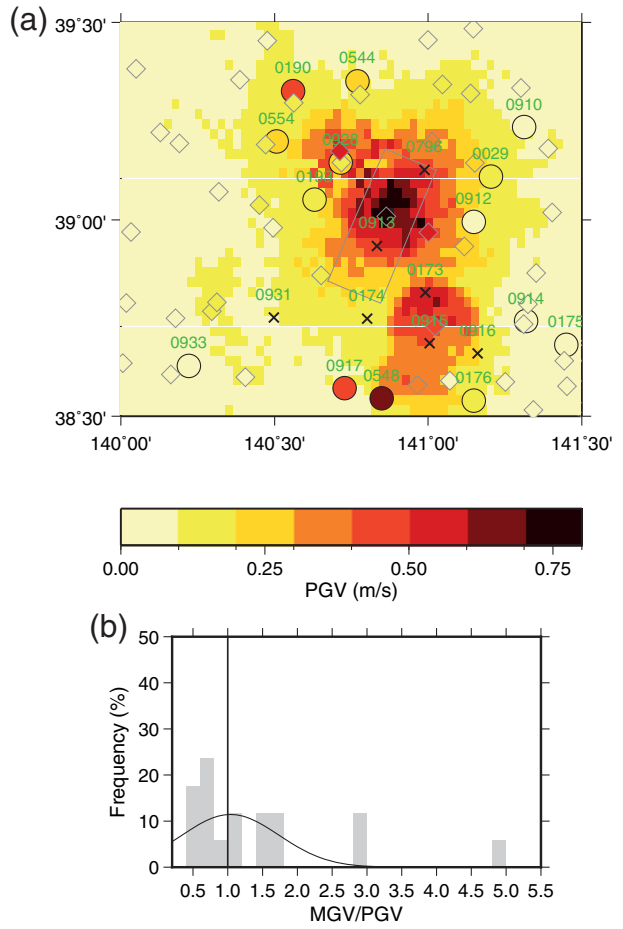

Figure 6. (a) U.S. Geological Survey ShakeMap of the M_w 6.9 Iwate–Miyagi Nairiku event and PGV from strong-motion stations (diamonds) compared to MGV derived from GPS (circles, station numbers provided). Crosses represent GPS stations that failed recording the event. The source extent is from Yokota *et al.* (2009). Good agreement between the ShakeMap and the GPS dataset suggests that the GPS data could have been integrated in a postprocessed version. (b) Distribution of the MGV/PGV ratio for the available GPS stations. The fitted distribution uses the median and the L1 norm. The color version of this figure is available only in the electronic edition.

ability (τ) for PGV is about 0.3–0.4 (natural logarithm) according to recent GMPEs (Douglas and Edwards, 2016), which corresponds to a variability (one standard deviation) of ±35%–50%. It means that biases of 10% or 20%, although systematic toward lower values, are not large compared to the expected variability of PGV for a single event at a given distance from the source.

As already shown in Figure 3, events of magnitude 5.5 are poorly recorded by GPS, whereas events of magnitude 6 can be partly recorded in the near field (Fig. 5). Low ratios (below 60%) are retrieved for events of magnitude 6.5 and lower at distances from 10 km onward. The PGV is however well retrieved (nearly 80% at short distances, 50% at 100 km) for events of magnitude 7 and above. The effect of distance is less pronounced for these events, which means that a whole GPS network would record a high percentage of PGV, not only very close stations. Figure 5 also clearly shows that PGV is even more challenging to recover when recording at a 1 Hz sampling rate only: a significant decrease in PGV is noticed at short distances, up to 40 km for M_w 7.5 events, resulting in a saturating or even increasing MGV/PGV ratio with distance.

Observations from the 2008 Iwate–Miyagi Nairiku Earthquake

The 2008 M_w 6.9 Iwate–Miyagi Nairiku event has been recorded by GEONET stations up to 200 km from the epicenter (Yokota *et al.*, 2009; Hobiger *et al.*, 2012; Lucca *et al.*, 2012). According to our model, GPS can well record such an event up to about 100 km (Fig. 3). Unfortunately, no data are available for the two stations (0913, 0796) closest to the epicenter due to a communication-line outage. We processed the data available in the area following the strategy defined by Houlié *et al.* (2011) that allows describing both static and dynamic motions associated with a seismic wavefield (Houlié *et al.*, 2014). We show the comparison of computed MGV from GPS data with the PGV from the U.S. Geological Survey ShakeMap produced using strong-motion data within hours following the event in the first 50 km (Fig. 6). GPS data collected by the GEONET enable us to compute GPS-based MGV values that could have contributed to the ShakeMap. A comparison of the GPS MGV with the ShakeMap PGV values in Figure 6b shows that on average the difference between the two datasets is about 25% although some outliers exist. According to Figure 5, about 60% or more of the PGV is retrieved in the first 50 km for an event of this magnitude, which is consistent with the observations.

Conclusions

We showed that GPS is able to provide critical data at intermediate to long periods ($T > 0.5$ s) for hazard assessment although the current standard sample rate for GPS is only 1 Hz (Nyquist period of 2 s). A useful estimate of PGV can even be retrieved for large earthquakes ($M_w > 7$). Given current processing techniques, the standard GPS sampling rate of 1 Hz is sufficient for far-field recordings of earthquakes. Higher sampling rates (5 Hz or more) would, however, be required to record all possible on-scale energy for near-field records (i.e., for stations located within a 10-km epicentral distance for magnitude 6 events and within 30 km for magnitude 7) and for megathrust earthquakes at larger distances. This higher sampling rate is particularly crucial to retrieve more accurate estimates of PGV in the near field. We find that using sampling rates above 5 Hz does not provide any additional information for earthquake ground-motion recordings except at very short distances (below 5 km). This is true even using more accurate postprocessed methods. PGV values (especially those extracted using postprocessed data) can complement PGV datasets from seismo-

logical stations when developing ground-motion models, especially for large events where GPS data are available at short distances. Moreover, real-time GPS processing methods such as PPP would allow integration of high-rate GPS data in near-real-time seismological products such as ShakeMap.

Given the density of the local GPS networks, we can expect GPS receivers to start recording events with $M_w > 5.8$ for station spacing of 30 km, as is the case in Switzerland and Japan. Those performances can be achieved even in real time using either RTK or PPP processing strategies. This value can go down to $M_w > 5.6$ in Switzerland in postprocessing mode. The usefulness of GPS in real-time monitoring can be improved by reducing the difference in displacement resolution between real-time and postprocessed GPS data (currently greater than one order of magnitude), and the multipath environment (an order of magnitude within RTK accuracies).

The variability of ground motion (assumed to be covered by an SNR of 3 in this study) imposes an additional uncertainty on the capabilities of GPS in terms of magnitude and distance. Our results should therefore be taken with care: the designer of a GPS network should account for this variability when using the provided numbers. However, this study indicates the scale of what can be achieved on average with GPS recordings.

Modern strong-motion stations installed with high care to avoid site failure and consequent tilting can reach a better noise performance than GPS up to 50 s. In countries with moderate seismicity like Switzerland, it may therefore be worth investing in such high-quality strong-motion installations (Michel *et al.*, 2014). In regions with high seismicity, it is clearly worthwhile to collocate strong-motion stations with high-rate GPS, especially at soft sediment sites, to ensure the recording of the entire wavefield. In any region, real-time high-rate GPS displacement records have a clear potential to be used in earthquake early warning.

Data and Resources

Global Positioning System (GPS) data of Japan were acquired through Geographical Survey Institute (GSI) of Japan from http://datahouse1.gsi.go.jp/terras/terras_english.html (last accessed June 2016). RTNet 1 Hz GNSS Earth Observation Network System (GEONET) data are provided by the Geospatial Information Authority of Japan via the Nippon GPS Data Services Company. Processed results were made available online at http://www.rtgps.com/rtnet_pppar_honshu_eq.php (last accessed June 2016). U.S. Geological Survey ShakeMap of the Iwate event was downloaded from https://earthquake.usgs.gov/earthquakes/eventpage/usp000g9h6#shakemap (last accessed June 2016). GIPSY software can be obtained from https://gipsy-oasis.jpl.nasa.gov (last accessed January 2017).

Acknowledgments

The acquisition of Global Positioning System (GPS) data of Japan has been possible due to Swiss National Science Foundation (SNSF) support. Very high-rate GPS data in Greece were collected during a campaign supported by CH-SNF (SNF 200021_143605). The authors are also grateful to Associate Editor Eric Chael, Markus Rothacher, and two anonymous reviewers who helped significantly improve the article.

References

Akkar, S., M. A. Sandikkaya, and J. J. Bommer (2014). Empirical ground-motion models for point- and extended-source crustal earthquake scenarios in Europe and the Middle East, *Bull. Earthq. Eng.* **12,** 359–387.

Allen, R. M., and A. Ziv (2011). Application of real-time GPS to earthquake early warning, *Geophys. Res. Lett.* **38,** L16310, doi: 10.1029/2011GL047947.

Anderson, J. G., and S. E. Hough (1984). A model for the shape of the Fourier amplitude spectrum of acceleration at high-frequencies, *Bull. Seismol. Soc. Am.* **74,** 1969–1993.

Atkinson, G. M., and K. Assatourians (2015). Implementation and validation of EXSIM (a stochastic finite-fault ground-motion simulation algorithm) on the SCEC broadband platform, *Seismol. Res. Lett.* **86,** no. 1, 48–60.

Atkinson, G. M., and I. Beresnev (1997). Don't call it stress drop, *Seismol. Res. Lett.* **68,** 3–4.

Atkinson, G. M., and D. M. Boore (2006). Earthquake ground-motion prediction equations for eastern North America, *Bull. Seismol. Soc. Am.* **96,** 2181–2205.

Atkinson, G. M., K. Assatourians, D. M. Boore, K. Campbell, and D. Motazedian (2009). A guide to differences between stochastic point-source and stochastic finite-fault simulations, *Bull. Seismol. Soc. Am.* **99,** 3192–3201.

Avallone, A., M. Marzario, A. Cirella, A. Piatanesi, A. Rovelli, C. Di Alessandro, E. D'Anastasio, N. D'Agostino, R. Giuliani, and M. Mattone (2011). Very high rate (10 Hz) GPS seismology for moderate-magnitude earthquakes: The case of the M_w 6.3 L'Aquila (central Italy) event, *J. Geophys. Res.* **116,** no. B2, doi: 10.1029/2010JB007834.

Bilich, A., J. F. Cassidy, and K. M. Larson (2008). GPS seismology: Application to the 2002 M_w 7.9 Denali fault earthquake, *Bull. Seismol. Soc. Am.* **98,** no. 2, 593–606.

Bock, Y., D. Melgar, and B. W. Crowell (2011). Real-time strong-motion broadband displacements from collocated GPS and accelerometers, *Bull. Seismol. Soc. Am.* **101,** no. 6, 2904–2925.

Bommer, J. J., and J. E. Alarcon (2006). The prediction and the use of peak ground velocity, *J. Earthq. Eng.* **10,** 1–31.

Bommer, J. J., B. Dost, B. Edwards, P. J. Stafford, J. van Elk, D. Doornhof, and M. Ntinalexis (2016). Developing an application-specific ground-motion model for induced seismicity, *Bull. Seismol. Soc. Am.* **106,** 158–173.

Boore, D. M. (2003). Analog-to-digital conversion as a source of drifts in displacements derived from digital recordings of ground acceleration, *Bull. Seismol. Soc. Am.* **93,** no. 5, 2017–2024.

Boore, D. M. (2009). Comparing stochastic point-source and finite-source ground-motion simulations: SMSIM and EXSIM, *Bull. Seismol. Soc. Am.* **99,** 3202–3216.

Bradley, B. A. (2012). Empirical correlations between peak ground velocity and spectrum-based intensity measures, *Earthq. Spectra* **28,** 17–35.

Brune, J. N. (1970). Tectonic stress and the spectra of seismic shear waves from earthquakes, **75,** no. 26, 4997–5009.

Cauzzi, C., and J. Clinton (2013). A high- and low-noise model for high-quality strong-motion accelerometer stations, *Earthq. Spectra* **29,** 85–102.

Cauzzi, C., and E. Faccioli (2008). Broadband (0.05 to 20 s) prediction of displacement response spectra based on worldwide digital records, *J. Seismol.* **12,** 453–475.

Cauzzi, C., B. Edwards, D. Fäh, J. Clinton, S. Wiemer, P. Kästli, G. Cua, and D. Giardini (2015). New predictive equations and site amplification estimates for the next-generation Swiss ShakeMaps, *Geophys. J. Int.* **200,** 421–438.

Dach, R., S. Lutz, P. Walser, and P. Fridez (2015). *Bernese GNSS Software Version 5.2.*, University of Bern, Bern, Switzerland.

Delouis, B., J.-M. Nocquet, and M. Vallée (2010). Slip distribution of the February 27, 2010 $M_w = 8.8$ Maule earthquake, central Chile, from static and high-rate GPS, InSAR, and broadband teleseismic data, *Geophys. Res. Lett.* **37,** L17305, doi: 10.1029/2010GL043899.

Douglas, J., and B. Edwards (2016). Recent and future developments in earthquake ground motion estimation, *Earth Sci. Rev.* **160,** 203–219.

Dow, J. M., R. E. Neilan, and C. Rizos (2009). The International GNSS Service in a changing landscape of Global Navigation Satellite Systems, *J. Geodes.* **83,** no. 3, 191–198.

Drouet, S., and F. Cotton (2015). Regional stochastic GMPEs in low-seismicity areas: Scaling and aleatory variability analysis—Application to the French Alps, *Bull. Seismol. Soc. Am.* **105,** no. 4, 1883–1902.

Edwards, B., and D. Fäh (2013). A stochastic ground-motion model for Switzerland, *Bull. Seismol. Soc. Am.* **103,** 78–98.

Edwards, B., D. Fäh, and D. Giardini (2011). Attenuation of seismic shear wave energy in Switzerland, *Geophys. J. Int.* **185,** 967–984.

Edwards, B., C. Michel, V. Poggi, and D. Fäh (2013). Determination of site amplification from regional seismicity: Application to the Swiss national seismic networks, *Seismol. Res. Lett.* **84,** 611–621.

Edwards, B., V. Poggi, and D. Fäh (2011). A predictive equation for the vertical-to-horizontal ratio of ground motion at rock sites based on shear-wave velocity profiles from Japan and Switzerland, *Bull. Seismol. Soc. Am.* **101,** 2998–3019.

Faenza, L., and A. Michelini (2010). Regression analysis of MCS intensity and ground motion parameters in Italy and its application in ShakeMap, *Geophys. J. Int.* **180,** 1138–1152.

Fäh, D., D. Giardini, P. Kästli, N. Deichmann, M. Gisler, G. Schwarz-Zanetti, S. Alvarez-Rubio, S. Sellami, B. Edwards, B. Allmann, *et al.* (2011). *ECOS-09 Earthquake Catalogue of Switzerland Release 2011. Report and Database. Public Catalogue. Report No. SED/RISK/R/001/20110417*, Swiss Seismological Service, ETH Zurich, Zurich, Switzerland.

Genrich, J. F., and Y. Bock (2006). Instantaneous geodetic positioning with 10–50 Hz GPS measurements: Noise characteristics and implications for monitoring networks, *J. Geophys. Res.* **111,** no. B03403, doi: 10.1029/2005JB003617.

Goulet, C. A., N. A. Abrahamson, P. G. Somerville, and K. E. Wooddell (2015). The SCEC broadband platform validation exercise: Methodology for code validation in the context of seismic-hazard analyses, *Seismol. Res. Lett.* **86,** no. 1, 17–26.

Häberling, S., M. Rothacher, Y. Zhang, J. F. Clinton, and A. Geiger (2015). Assessment of high-rate GPS using a single-axis shake table, *J. Geodes.* **89,** no. 7, 697–709.

Hanks, T. C., and R. K. Mcguire (1981). The character of high-frequency strong ground motion, *Bull. Seismol. Soc. Am.* **71,** 2071–2095.

Hauksson, E., P. Small, K. Hafner, R. Busby, R. Clayton, J. Goltz, T. Heaton, K. Hutton, H. Kanamori, J. Polet, *et al.* (2001). Southern California Seismic Network: Caltech/USGS element of TriNet 1997–2001, *Seismol. Res. Lett.* **72,** no. 6, 690–704.

Herring, T., R. W. King, and S. M. McClusky (2015). *Introduction to GAMIT/GLOBK Release 10.6*, Massachusettes Institute of Technology, Cambridge, Massachusettes.

Hobiger, M., U. Wegler, K. Shiomi, and H. Nakahara (2012). Coseismic and postseismic elastic wave velocity variations caused by the 2008 Iwate–Miyagi Nairiku earthquake, Japan, *J. Geophys. Res.* **117,** no. B09313, doi: 10.1029/2012JB009402.

Houlié, N., D. Dreger, and A. Kim (2014). GPS source solution of the 2004 Parkfield earthquake, *Sci. Rep.* **4,** Article No. 3646.

Houlié, N., G. Funning, and R. Bürgmann (2016). Use of a GPS-derived troposphere model to improve InSAR deformation estimates in the San Gabriel Valley, California, *IEEE Trans. Geosci. Remote Sens.* **54,** no. 9, 5365–5374.

Houlié, N., G. Occhipinti, T. Blanchard, N. Shapiro, P. Lognonne, and M. Murakami (2011). New approach to detect seismic surface waves in 1 Hz-sampled GPS time series, *Sci. Rep.* **1,** Article No. 44.

Ibrahim, R., H. Si, K. Koketsu, and H. Miyake (2016). Long-period ground-motion prediction equations for moment magnitude estimation of large earthquakes in Japan, *Bull. Seismol. Soc. Am.* **106,** 54–72.

Jeon, S. S., and T. D. O'Rourke (2005). Northridge earthquake effects on pipelines and residential buildings, *Bull. Seismol. Soc. Am.* **95,** 294–318.

Kaloop, M. R., and M. Rabah (2016). Time and frequency domains response analyses of April 2015 Greece's earthquake in the Nile Delta based on GNSS–PPP, *Arab. J. Geosci.* **9,** no. 316, doi: 10.1007/s12517-016-2343-8.

Kelevitz, K., N. Houlié, D. Giardini, and M. Rothacher (2017). Performance of high-rate GPS waveforms at long periods: Moment tensor inversion of the 2003 M 8.3 Tokachi-Oki earthquake, *Bull. Seismol. Soc. Am.* doi: 10.1785/0120160338 (in press).

Konno, K., and T. Ohmachi (1998). Ground-motion characteristics estimated from spectral ratio between horizontal and vertical components of microtremor, *Bull. Seismol. Soc. Am.* **88,** 228–241.

Larson, K. M., and S. i. Miyazaki (2008). Resolving static offsets from high-rate GPS data: The 2003 Tokachi-oki earthquake, *Earth Planets Space* **60,** no. 8, 801–808.

Larson, K. M., P. Bodin, and J. Gomsberg (2003). Using 1-Hz GPS data to measure deformations caused by the Denali fault earthquake, *Science* **300,** 1421–1424.

Lay, T., Y. Yamazaki, C. J. Ammon, K. F. Cheung, and H. Kanamori (2011). The 2011 M_w 9.0 off the Pacific coast of Tohoku earthquake: Comparison of deep-water tsunami signals with finite-fault rupture model predictions, *Earth Planets Space* **63,** no. 7, 797–801.

Lesueur, C., M. Cara, O. Scotti, A. Schlupp, and C. Sira (2013). Linking ground motion measurements and macroseismic observations in France: A case study based on accelerometric and macroseismic databases, *J. Seismol.* **17,** 313–333.

Lucca, E., G. Festa, and A. Emolo (2012). Kinematic inversion of strong-motion data using a Gaussian parameterization for the slip: Application to the 2008 Iwate–Miyagi, Japan, earthquake, *Bull. Seismol. Soc. Am.* **102,** no. 6, 2685–2703.

Melgar, D., B. W. Crowell, J. Geng, R. M. Allen, Y. Bock, S. Riquelme, E. M. Hill, M. Protti, and A. Ganas (2015). Earthquake magnitude calculation without saturation from the scaling of peak ground displacement, *Geophys. Res. Lett.* **42,** no. 13, 5197–5205.

Michel, C., B. Edwards, V. Poggi, J. Burjánek, D. Roten, C. Cauzzi, and D. Fäh (2014). Assessment of site effects in Alpine regions through systematic site characterization of seismic stations, *Bull. Seismol. Soc. Am.* **104,** no. 6, 2809–2826.

Mitsui, Y., and K. Heki (2012). Observation of Earth's free oscillation by dense GPS array: After the 2011 Tohoku megathrust earthquake, *Sci. Rep.* **2,** Article No. 931.

Miyazaki, S., and K. M. Larson (2008). Coseismic and early postseismic slip for the 2003 Tokachi-oki earthquake sequence inferred from GPS data, *Geophys. Res. Lett.* **35,** no. 4, doi: 10.1029/2007GL032309.

Miyazaki, S., K. M. Larson, K. H. Choi, K. Hikima, K. Koketsu, P. Bodin, J. Haase, G. Emore, and A. Yamagiwa (2004). Modeling the rupture process of the 2003 September 25 Tokachi-Oki (Hokkaido) earthquake using 1-Hz GPS data, *Geophys. Res. Lett.* **31,** no. 21, doi: 10.1029/2004GL021457.

Motazedian, D., and G. M. Atkinson (2005). Stochastic finite-fault modeling based on a dynamic corner frequency, *Bull. Seismol. Soc. Am.* **95,** 995–1010.

Orense, R. P. (2005). Assessment of liquefaction potential based on peak ground motion parameters, *Soil Dynam. Earthq. Eng.* **25,** 225–240.

Poggi, V., B. Edwards, and D. Fäh (2011). Derivation of a reference shear-wave velocity model from empirical site amplification, *Bull. Seismol. Soc. Am.* **101,** no. 1, 258–274.

Poggi, V., B. Edwards, and D. Fäh (2013). Reference S-wave velocity profile and attenuation models for ground-motion prediction equations: Application to Japan, *Bull. Seismol. Soc. Am.* **103,** no. 5, 2645–2656.

Psimoulis, P., N. Houlié, M. Meindl, and M. Rothacher (2015). Consistency of GPS and strong-motion records: Case study of M_w 9.0 Tohoku-Oki 2011 earthquake, *Smart Syst. Struct.* **16,** no. 2, 347–366.

Psimoulis, P., N. Houlié, C. Michel, M. Meindl, and M. Rothacher (2014). Long-period surface motion of the multi-patch M_w 9.0 Tohoku-Oki earthquake, *Geophys. J. Int.* **199,** 968–980.

Rhie, J., D. S. Dreger, M. Murray, and N. Houlié (2009). Peak ground velocity ShakeMaps derived from geodetic slip models, *Geophys. J. Int.* **179,** no. 2, 1105–1112.

Rietbrock, A., F. Strasser, and B. Edwards (2013). A stochastic earthquake ground-motion prediction model for the United Kingdom, *Bull. Seismol. Soc. Am.* **103,** 57–77.

Rocken, C., L. Mervart, Z. Lukes, J. Johnson, H. Kanzaki, M. Kakimoto, and Y. Iotake (2004). Testing a new network RTK software system, *17th International Technical Meeting of the Satellite Division of the Institute of Navigation (ION GNSS 2004)*, Inst. of Navig., Fairfax, Virginia.

Shi, C., Y. Lou, H. Zhang, Q. Zhao, J. Geng, R. Wang, R. Fang, and J. Liu (2010). Seismic deformation of the M_w 8.0 Wenchuan earthquake from high-rate GPS observations, *Adv. Space Res.* **46,** no. 2, 228–235.

Smalley, R., Jr. (2009). Hi-rate GPS: How high do we need to go?, *Seismol. Res. Lett.* **80,** no. 6, 1054–1061.

Takasu, T., N. Kubo, and A. Yasuda (2007). Development, evaluation and application of RTKLIB: A program library for RTK-GPS, *GPS/GNSS Symposium 2007*, Tokyo, Japan, 20–22 November 2007 (in Japanese).

Welch, P. D. (1967). The use of fast Fourier transform for the estimation of power spectra: A method based on time averaging over short, modified periodograms, *IEEE Trans. Audio Electroacoust.* **15,** no. 2, 70–73.

Wells, D. L., and K. J. Coppersmith (1994). New empirical relationships among magnitude, rupture length, rupture width, rupture area, and surface displacement, *Bull. Seismol. Soc. Am.* **84,** 974–1002.

Worden, C. B., D. J. Wald, T. I. Allen, K. Lin, and D. Garcia (2010). A revised ground-motion and intensity interpolation scheme for ShakeMap, *Bull. Seismol. Soc. Am.* **100,** 3083–3096.

Yokota, Y., K. Koketsu, K. Hikima, and S. Miyazaki (2009). Ability of 1-Hz GPS data to infer the source process of a medium-sized earthquake: The case of the 2008 Iwate–Miyagi Nairiku, Japan, earthquake, *Geophys. Res. Lett.* **36,** no. 12, doi: 10.1029/2009GL037799.

Yue, H., and T. Lay (2011). Inversion of high-rate (1 sps) GPS data for rupture process of the 11 March 2011 Tohoku earthquake (M_w 9.1), *Geophys. Res. Lett.* **38,** no. 7, doi: 10.1029/2011GL048700.

Zhao, J. X., J. Zhang, A. Asano, Y. Ohno, T. Oouchi, T. Takahashi, H. Ogawa, K. Irikura, H. K. Thio, P. G. Somerville, *et al.* (2006). Attenuation relations of strong ground motion in Japan using site classification based on predominant period, *Bull. Seismol. Soc. Am.* **96,** no. 3, 898–913.

Zheng, Y., J. Li, Z. Xie, and M. H. Ritzwoller (2012). 5 Hz GPS seismology of the El Mayor Cucapah earthquake: Estimating the earthquake focal mechanism, *Geophys. J. Int.* **190,** 1723–1732.

Swiss Seismological Service (SED)
ETH Zurich
Sonneggstrasse 5
8092 Zürich, Switzerland
clotaire.michel@sed.ethz.ch
(C.M., J.C.)

Institute of Geophysics (SEG)
ETH Zurich
Sonneggstrasse 5
8092 Zürich, Switzerland
(K.K., N.H., D.G.)

Department of Earth, Ocean and Ecological Sciences
University of Liverpool
Jane Herdman Building, 4 Brownlow Street
Liverpool L69 3GP, United Kingdom
(B.E.)

Department of Civil Engineering
University of Nottingham
Nottingham Geospatial Building, Jubilee Campus, Wollaton Road
Nottingham NG8 1BB, United Kingdom
(P.P.)

Mathematical Physical Geodesy (MPG)
ETH Zurich
Robert-Gnehm-Weg 15
8093 Zürich, Switzerland
(Z.S.)

Manuscript received 23 September 2016;
Published Online 16 May 2017